Energy 94 (2016) 250–261

Contents lists available at ScienceDirect

Energy

journal homepage: www.elsevier.com/locate/energy

Experimental and numerical studies of hybrid PCM embedded in plastering mortar for enhanced thermal behaviour of buildings

Mohammad Kheradmand [a, *], Miguel Azenha [b, 1], José L.B. de Aguiar [a, 2], João Castro-Gomes [c, 3]

[a] CTAC – Territory, Environment and Construction Research Centre, University of Minho, School of Engineering, Civil Engineering Dept., Azurém Campus, 4800-058 Guimarães, Portugal
[b] ISISE – Institute for Sustainability and Innovation in Structural Engineering, University of Minho, School of Engineering, Civil Engineering Dept., Azurém Campus, 4800-058 Guimarães, Portugal
[c] C-MADE, Centre of Materials and Building Technologies, Department of Civil Engineering and Architecture, University of Beira Interior, 6201-001 Covilhã, Portugal

ARTICLE INFO

Article history:
Received 21 May 2015
Received in revised form
29 September 2015
Accepted 28 October 2015
Available online xxx

Keywords:
Hybrid PCM
Plastering mortar
Energy efficiency
Façade
Buildings

ABSTRACT

This paper proposes a methodology for improvement of energy efficiency in buildings through the innovative simultaneous incorporation of three distinct phase change materials (here termed as hybrid PCM) in plastering mortars for façade walls. The thermal performance of a hybrid PCM mortar was experimentally evaluated by comparing the behaviour of a prototype test cell (including hybrid PCM plastering mortar) subjected to realistic daily temperature profiles, with the behaviour of a similar prototype test cell, in which no PCM was added. A numerical simulation model was employed (using ANSYS-FLUENT) to validate the capacity of simulating temperature evolution within the prototype containing hybrid PCM, as well as to understand the contribution of hybrid PCM to energy efficiency. Incorporation of hybrid PCM into plastering mortars was found to have the potential to significantly reduce heating/cooling temperature demands for maintaining the interior temperature within comfort levels when compared to normal mortars (without PCM), or even mortars comprising a single type of PCM.

1. Introduction

Nowadays, there is significant interest in the application of innovative technologies to improve the energy efficiency of buildings, particularly due to increasing concerns about energy sustainability and even global climatic changes [1]. In fact, buildings consume more than a third of the world's energy [2], which is directly linked to the rate of growth in the population and the corresponding increase of energy demand for indoor thermal comfort. Therefore, it is relevant to develop materials/techniques that can help maintaining indoor temperatures within comfort levels, while assisting in the reduction of energy consumption for such purpose.

One potential methodology for enhancing the thermal behaviour of buildings is the use of thermal energy storage materials, such as PCMs (phase change materials), which are relatively easy to incorporate into building components. The principle of operation of PCMs in the scope of building physics can be explained by an example in which PCM is used as a part of the construction of a façade: when subjected to temperatures in excess of its melting temperature range, the PCM absorbs heat by changing from the solid to the liquid state, thus delaying the flux of heat towards the interior of the building. Conversely, the stored heat is released when the temperature drops below the solidification temperature range of the PCM. This leads to better levelled indoor temperatures, that tend to be in the vicinity of the PCM's melting point, but also has the interesting feature of shifting the building heating/cooling load from peak to off-peak electricity consumption periods [3].

Several studies have investigated the use of different types of PCMs applied in the context of buildings, such as: copolymer

* Corresponding author. Tel.: +351 913542324; fax: +351 253 510 217.
E-mail addresses: mohammadkheradmand@hotmail.com (M. Kheradmand), miguel.azenha@civil.uminho.pt (M. Azenha), aguiar@civil.uminho.pt (J.L.B. de Aguiar), castro.gomes@ubi.pt (J. Castro-Gomes).
[1] Tel.: +351938404554; fax: +351 253 510 217.
[2] Tel.: +351 253 510 206; fax: +351 253 510217.
[3] Tel.: +351 275 329 990; fax: +351 275 329 969.

http://dx.doi.org/10.1016/j.energy.2015.10.131
0360-5442/

Nomenclature

$C_{specimen}$	Specific heat capacity of the specimen (J/kg K)
C_{PCM}	Specific heat capacity of the PCM (J/kg K)
W_{PCM}	Weight ratio of the PCM to the specimen
C_{mortar}	Specific heat capacity of the plain material (J/kg K)
W_{mortar}	Mass fraction of the plain mortar
U	Thermal transmittance (W/m^2 K)
$T_{Sol-Air}$	Sol–air temperature (°C)
T_{Air}	Exterior temperature (°C)
α	Absorption coefficient of the surface
I_g	Global solar radiation (W/m^2)
R_{se}	External surface resistance ((m^2 K)/W)
ρ	Density of the material (kg/m^3)
$C(T)$	Temperature dependent of specific heat capacity (J/kg K)
T	Static temperature (°C)
k	Thermal conductivity (W/m K)
$DSC(T)_s$	The heat flow across the specimen at temperature T from the thermogram (m W/mg)
φ	Heating rate (°C/s)
Δt	Time step (s)
q	Heat flow (W/m)
h_{eq}	Convection/radiation coefficient (W/m K)
T_s	Surface temperature (°C)
C_p	Specific heat capacity (J/kg K)
I	Thermal inertia (J/m^2 K s$^{1/2}$)
T	Time (h)

composite [4]; epoxy resin/paraffin spheres [5], tiles [6] plastering mortars [7], ceiling panels [8], bricks [9], shape-stabilized PCMs [10], etc.

Incorporation of PCM into plastering mortars of building facades can improve thermal efficiency of buildings due to their ability to store energy and it allows to reduce the energy consumption of heating/cooling systems used to control the indoor temperature of the room. The incorporation of PCM in mortar or concrete has shown promising results through lower thermal conductivity and increased thermal mass [11,12]. It has also been demonstrated that the incorporation of PCM's into plastering mortars does not impair their relevant mechanical performance, particularly in regard to shrinkage cracking sensitivity [13]. PCMs are inert materials, and PCM in cement based materials have been observed to show significant stability after exposure to temperatures well above those of natural environment by not exhibiting signs of degradation up to about 200 °C [14], as well as no ignition/flammability at such temperature range [11]. The embedment of PCMs in mortars has been reported to induce flames when heated to 1000 °C [15]. Nevertheless, PCM mortars have shown potential of self-extinguish of the flame when the heat source is removed, which is a very positive sign in terms of flame spreading potential in the case of fire [15].

It is further remarked that the conduction of accurate simulations of the transient thermal behaviour of mortar with incorporated PCM is relevant subject which has been identified as requiring conclusive research outcomes [16], as to allow sound prediction and optimization of PCM mortar mixes.

Recent research efforts on behalf of the authors of this research work have been focused on the possibility of using more than one type of PCM (with distinct melting ranges and specific enthalpies) in the same plastering mortar for improvement of the effectiveness of the PCM-based system [17]. However, such possibility (here termed as hybrid PCM), was solely assessed at the material level in what concerns to homogeneity distribution of different materials matrices within plastering mortar and the behaviour of hybrid PCM's under DSC (Differential Scanning Calorimetry) testing. Based on the promising results of such previous works, the present paper focuses on experimental and numerical testing of the hybrid PCM concept applied to mortars. Small scale prototypes have been tested and simulated under realistic daily temperature histories. In fact, the presence of a wider temperature range in which the phase changes take place can potentially increase global performance and versatility of the PCM-based system.

In order to provide deeper knowledge about the advantages of using more than one type of PCM in the same plastering mortar, and relate the resulting behaviour to that of a reference mortar (without PCM), the experimental program of this research work focused on both types of mortar formulation. The experiments were preceded by a detailed material characterization of the mortars involved, namely the thermal conductivity and the thermal behaviour by DSC (differential scanning calorimetry). The hybrid PCM, containing three distinct types of PCMs, was incorporated into a plastering mortar which was in turn applied as render on extruded polystyrene (XPS) panels that composed the outer walls of a hollow cube, here termed as 'laboratory scale prototype'. A similar hollow cube was produced using the reference mortar as coating material. The two cubic prototypes were placed inside a climatic chamber and subjected to simulated real temperature variations, thus allowing to evaluate the differences in thermal performance induced by the two types of tested mortars. A numerical simulation of the experiments was performed with the intent of better understanding the effects of hybrid PCM on the thermal behaviour and to gain confidence in the modelling approaches (i.e. validation). This paves the way for the feasibility of future conduction of numerical sensitivity studies based on the lessons learnt from the experiments.

2. Experimental work

2.1. Materials and formulations

2.1.1. Choice of PCMs for incorporation

The choice of the melting temperature of the PCMs for incorporation should be anchored in a combination of the intended thermal comfort range together with the typical climatic conditions of the location of the building. In Southern European countries (such as Portugal), the maximum sol-air temperature may reach 44 °C in a typical summer day while, the minimum sol-air temperature typically reaches to 5 °C during the winter season [18]. Hence, the initial selection of materials for this research was limited to those exhibiting phase change in the temperature range of 10–30 °C, which covers the sol-air temperature variations mentioned above for both winter and summer periods in Portugal. Microencapsulated PCMs have shown adequate advantages over bulk PCM because they prevent leakage during solid–liquid phase change, and also provide higher heat transfer area per unit volume [19]. The selection of PCMs also took into account chemical compatibility with inorganic materials and the range of available PCM products available in the market [20].

Based on the reasoning made so far, four types of paraffin-wax-based organic PCMs were considered for the experimental program reported herein: RT10 with melting temperature of 10 °C (from RUBITHERM paraffin RT series), MC28 with melting temperature of

28 °C, MC24 with melting temperature of 24 °C (from DEVAN microencapsulated MC series) and BSF26 with melting temperature of 26 °C (from BASF microencapsulated Micronal series DS 5001). The properties of the PCMs selected for this study, as provided by their suppliers [21–23], are presented in Table 1.

2.1.2. Mortar formulations

According to previous developments of this research team [17], the formulation of mortars with incorporation of microencapsulated PCM allowed the mass fraction of PCM to reach nearly 20% of the global mass of the mortar. In spite of such high incorporation level, the performance in terms of several properties of the mortar was maintained at satisfactory levels, namely in regard to: workability, compressive strength, flexural strength and adhesion [13]. The mix designs of the two mortars studied herein, together with their adopted designations (REFM for the reference mortar and HPCMM for the hybrid PCM mortar) are presented in Table 2. It should be noted that, the formulation of mortars HPCMM adopted herein comprises three distinct PCMs, as opposed to previous works of this research team in which only two distinct PCMs had been used [17]. The HPCMM studied incorporates a combination of three PCMs with melting temperatures of 10 °C, 26 °C and 28 °C. The choice of these three specific PCMs, as well as their relative proportions, was based on a preliminarily set of sensitivity numerical simulations of the thermal behaviour of the prototypes, which are here omitted for the sake of brevity/continuity. These three PCMs are placed in equal mass quantity, thus globally reaching 18.34% of weight within the mortar. Portland cement type I class 42.5R is adopted as binder. Industrial sand with mean particle size around 440 μm was used as inert filler. The detailed grain size distribution of the sand can be found in Ref. [17]. The mortars were mixed according to the procedures recommended by EN 1015:3 [24].

Experimental limitations led to the impossibility of testing a mortar containing a single PCM in the scope of this research work. Even though this was a undesirable situation, it is not seen as truly problematic, as the authors have been involved in previous research works in which numerical simulation of single PCM mortars has been achieved successfully [25], thus rendering comparison of performance of the hybrid PCM mortars with single PCM mortars to the stage of sensitivity numerical simulations presented herein.

2.2. Characterization and classification of materials

The main goal of the material characterization was to identify the necessary thermal and physical properties for use in the numerical simulations.

The main thermo-physical properties of the materials used in both prototypes, REFM and HPCMM, are synthetized on Table 3 and are detailed next. This table also contains information about the plates of XPS (extruded polystyrene) that were used in the construction of the prototype walls, according to information provided by the supplier [26].

Table 2
Mix proportions of formulations REFM and HPCMM.

Materials	Formulations (percentage of the total weight of mortar)	
	REFM	HPCMM
Cement type I-42.5R (SECIL)	22.64	31.32
Sand	64.23	30.59
Water	12.45	18.79
Super plasticizer	0.63	0.94
RT10	–	6.12
BSF26	–	6.12
MC28	–	6.12

2.2.1. Dry density

In order to determine dry densities of the mortars, a total number of 4 specimens were deployed for each mortar mix. The testing recommendations of EN1015:10 [27] were followed. Firstly, the specimens were formed into several cubes (with the dimensions of 50 mm × 50 mm × 50 mm). Then the specimens were kept sealed with a plastic sheet under at laboratory environment for about 24 h. After that, all specimens were submerged at 20 ± 1 °C for 7 days. Then, the cubes were dried at 70 °C until constant weight was reached. The accurate dimensions of the cubes were measured using a digital calliper with a precision of 0.02 mm, and their weights were measured using an analytical balance with a precision of 0.001 g. Dry density was then calculated directly.

Regarding the density difference between REFM and HPCMM, it is interesting to note that the density of HPCMM is only approximately 86% of that of REFM. In fact, the smaller density of HPCMM was expectable in view of the relevance of PCMs in the mix (which have low densities themselves).

2.2.2. Thermal conductivity

The thermal conductivities of the mortars were determined in four representative specimens of each mortar mix. The measurements were carried out through a steady state heat flow metre apparatus (ALAMABETA, model Sensora), according to ISO8301:1991 [28]. Mortars were casted into cylinder moulds with diameter of 0.1 m and length of 0.01 m respectively, which were sealed and cured for 28 days at 20 °C. Each test specimen is placed between two parallel plates set at distinct temperatures, whereas the steady-state heat flux is measured. The thermal conductivity of the specimen is calculated using Fourier's law of heat conduction according to [29].

The observed thermal conductivity of HPCMM (0.3 W/m K) is significantly lower than that of REFMM (0.4 W/m K) can induce a better insulating thermal behaviour of HPCMM in building envelopes, which accumulates with the advantages related to the energy storage of the PCM.

2.2.3. Specific heat capacity

The determination of specific heat capacities of the mortar specimens was performed through DSC testing (NETZSCH 200 F3 Maia), following the methodology recommended by ISO 11357:1

Table 1
Properties of PCMs, provided by suppliers [21–23].

PCM type	Operating temperature ranges (°C)	Latent heat of fusion (J/kg)	Melting point(°C)	Apparent density at solid state (kg/m^3)	Particle size distribution range (μm)
RT10	2–12	150,000	10	880	–
MC24	12–25	162,400	24	[a]	14–24
BSF26	10–30	110,000	26	350	5–90
MC28	22–32	170,100	28	[a]	14–24

[a] No information available on behalf of the suppliers.

Table 3
Thermo-physical properties of the materials used in REFM and HPCMM prototypes.

Thermo-physical properties	Ab.	Units	REFM (internal coating)	HPCMM (internal coating)	XPS (external coating)
Density	ρ	[kg/m^3]	1529.5	1309.8	32
Thermal conductivity	k	[W/m K]	0.4	0.3	0.034
Specific heat capacity	C_p	[J/kg K]	see Fig. 1	see Fig. 1	1400

[30]. One specimen was prepared for each type of mortar (REFM and HPCMM). The specimen preparation for DSC testing followed the methodology detailed in Ref. [17]. The weight of the prepared specimens was 24 mg and 37.88 mg, for REFM and HPCMM, respectively. A low heating rate of 1°Cmin^{-1} was considered for all experiments [31]. The applied program steps for the test procedure of specimens were the following: (i) initial isothermal period at 0 °C for 5 min; (ii) dynamic heating up to 40 °C according to the proposed rate (1 °C min^{-1}).

Fig. 1 presents specific heat capacity curves obtained for REFM and HPCMM. From such figure, it can be confirmed that the PCMs held their characteristics when incorporated into mortar mixture: in fact, the DSC thermogram of HPCMM reveals three peaks corresponding to the three embedded PCMs. However, it can be observed that the peak temperature of the RT10 in HPCMM shifted about 6 °C above the expectable peak according to the manufacturer (10 °C). The peak temperatures of the BSF26 and MC28 in HPCMM were shifted by nearly −2 °C. The reason for these deviations can be partly attributed to the dependency of results on the heating rate and the mass of the specimen in DSC testing, as shown in Ref. [32].

In order to better compare the thermal performance of both mortars, their thermal inertia was calculated according to Eq. (1) [33]:

$$I = \sqrt{\rho \times C_p \times k} \quad (1)$$

The results of such computation are shown in Fig. 2. It can be seen that the thermal inertia of HPCMM is higher than that of REFM for the majority of the studied temperatures, thus highlighting its higher potential in better attenuating the effects of external environmental temperatures in buildings. In fact, with a higher thermal inertia, a given material can be thermally activated faster and consequently, more thermal load can be stored during the dynamic thermal process [33].

2.3. Design and fabrication of the prototypes

In order to assess the effect of embedding hybrid PCMs into plastering mortars used as internal coatings for buildings, two laboratory-scale prototypes were built. These prototypes consisted in hollow boxes whose outer walls were materialized by polystyrene panels internally coated with the mortars under study. The materials used for the construction of the prototypes were (from inside to outside): a 0.02 m thick layer of REFM or HPCMM, and a 0.03 m thick of extruded polystyrene (XPS). The schematic diagram of prototypes with outer dimensions of 46 cm × 46 cm × 46 cm is shown in Fig. 3. The composition of the walls of the test cell is not a typical one in building envelopes. In fact, the target in this case was to have a small-sized prototype, with relatively thin walls, which would however have a thermal transmittance ($U \approx 0.89$ W/m^2 K) lower than the maximum limit according to Portuguese regulations for vertical elements (of $U = 1.45$ W/m^2 K) [34], thus having a reasonably similar thermal behaviour to actual building envelopes. In regard to temperature monitoring, PT100 sensors, with 0.1 °C accuracy, were positioned at the geometrical centre of the internal hollow region, with the final intention of monitoring internal temperature variations within the prototypes.

2.4. Thermal performance of prototypes

Each prototype was placed inside a controlled climatic chamber with inner dimensions of 1.04 m × 1.2 m × 0.6 m. The climatic chamber was programmed to follow temperature cycles that matched the sol–air temperature for a vertical wall facing south, located in the north of Portugal, with consideration of two distinct seasonal scenarios: summer and winter.

The sol-air temperature ($T_{Sol-Air}$) was computed according to Eq. (2) [25]:

$$T_{Sol-Air} = T_{Air} + \alpha I_g R_{se} \quad (2)$$

T_{Air} is the exterior temperature (°C); α is the absorption coefficient of the surface; I_g is the global solar radiation (W/m^2); and R_{se} is the external surface resistance ((m^2 K)/W). The values of exterior temperature (T_{Air}) and global solar radiation (I_g) were considered regarding average hourly values recorded for representative days of summer and winter in northern Portugal (Guimarães), obtained from a weather station located within the campus of the University

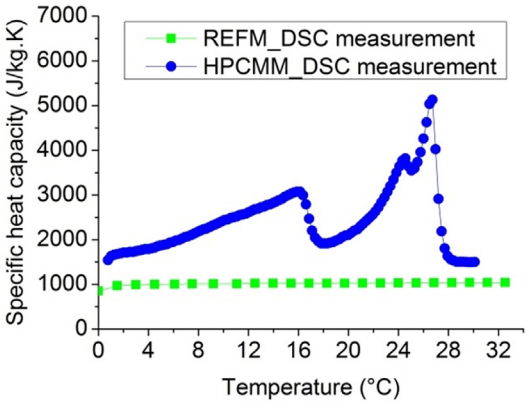

Fig. 1. DSC results for specific heat capacities of REFM and HPCMM.

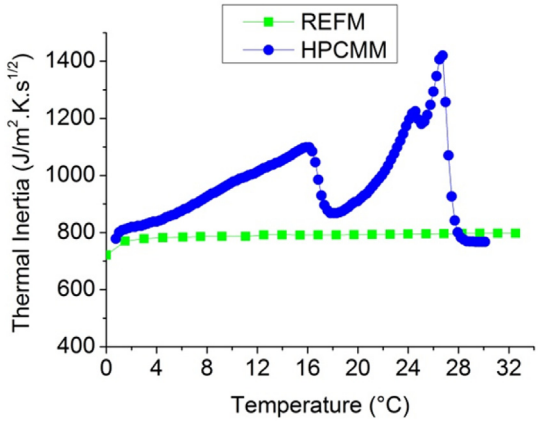

Fig. 2. Thermal inertia of mortars (REFM and HPCMM) in function of temperature.

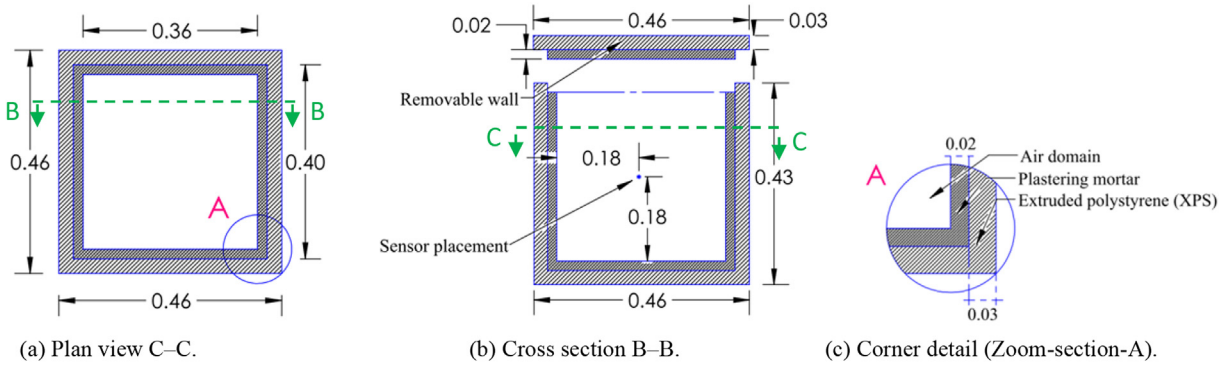

Fig. 3. Schematic representation and sensor placement of the prototypes. Units: [m].

of Minho. An absorption coefficient $\alpha = 0.6$ was considered in correspondence to colour of the surface material (XPS) [35]. The value of external surface resistance was adopted as $R_{se} = 0.04$ (m^2 K)/W in accordance to the recommendations of ISO 6946 [35]. As a result of the application of the sol–air temperature model, the 24 h cycles shown in Fig. 4 were obtained for summer and winter scenarios.

A total of four experiments were conducted by submitting the two prototypes (REFM and HPCMM) to the two environmental conditions (summer and winter), with each experiment lasting three full cycles (72 h). The climatic chamber in which the test was conducted also allowed the control of internal relative humidity, which was set to the constant value of RH = 50% throughout all the performed experiments. The physical arrangement of this setup can be observed at the pictures of the prototype/monitoring shown in Fig. 5. The readings of temperature sensors placed within the prototypes were collected through a computer-based data acquisition system (AGILENT 34970A) with a rate of one measurement per minute during whole period of testing.

2.5. Temperature monitoring results

The monitored temperatures for both prototypes under summer day conditions are shown in Fig. 6. It can be observed that the daily temperature amplitude inside the REFM prototype was of 13 °C (between 33 °C and 20 °C), whereas the HPCMM prototype endured a smaller internal temperature amplitude of 8.9 °C (between 31.5 °C and 22.6 °C). The difference in the minimum temperature recorded within the two prototypes is 22.6°C–20 °C = 2.6 °C, which is reasonably consistent with the observations of Vaz Sá et al. [25], who observed temperature differences of 2–3 °C in laboratory scale prototypes internally coated with mortar with a single PCM and without PCM. In the present study, the use of a hybrid PCM blend also allowed significant differences in the maximum peak temperatures: 1.5 °C difference between REFM and HPCMM prototypes confirming that HPCMM can also assist temperature regulation in this range. The delay between the maximum temperatures registered inside climatic chamber and inside the HPCMM prototype was of nearly 4.5 h, in opposition to a smaller delay of ~3 h associated to the REFM prototype.

It is interesting to note that, the minimum temperature achieved on the HPCMM prototype is mostly close to the phase transition of BSF26 and MC28 (see the DSC measurements in Fig. 1). The collected results for this summer scenario revealed that hybrid PCM acts by reducing inside temperature amplitudes during the day, levelling them and turning them closer to comfort temperature levels (around 24 °C). All this has occurred in spite of the fact that the RT10 PCM embedded in HPCMM was never activated within this summer scenario. It is also worth remarking that the differences in behaviour were not only caused by the energy storage effect. Indeed, the HPCMM had a slightly smaller thermal conductivity that (see Table 3) has also contributed to reduce heat fluxes inwards and outwards the prototype. Nonetheless, the HPCMM also had a relevant downside to overcome: as it is density was smaller than that of REFM (see Table 3), its volumetric heat capacity could have been reduced to an extent that might have been detrimental to its performance. That was not the case due to the increased specific heat of HPCMM (as shown in Fig. 1) that compensated for its lesser density.

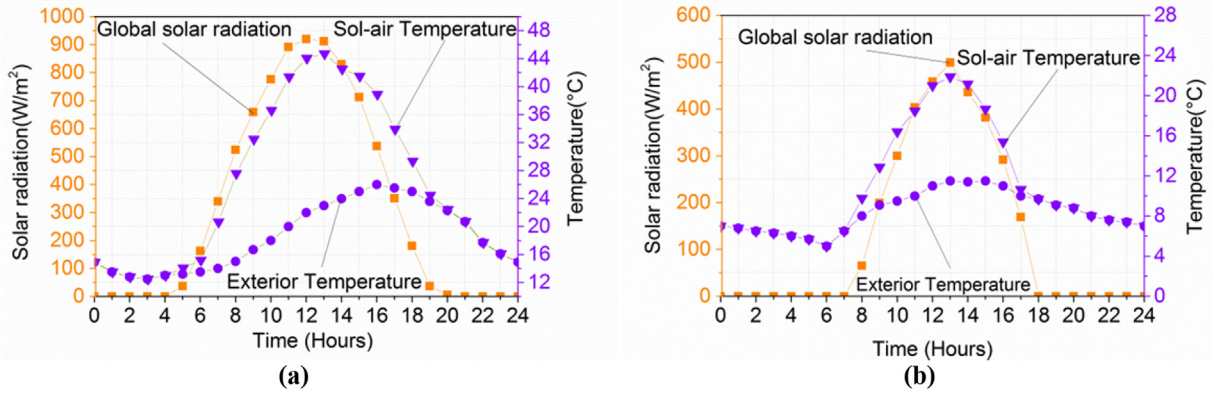

Fig. 4. Exterior temperature, solar radiation and sol–air temperature (south-oriented wall) for: (a) a summer day and (b) a winter day in Guimarães, Portugal.

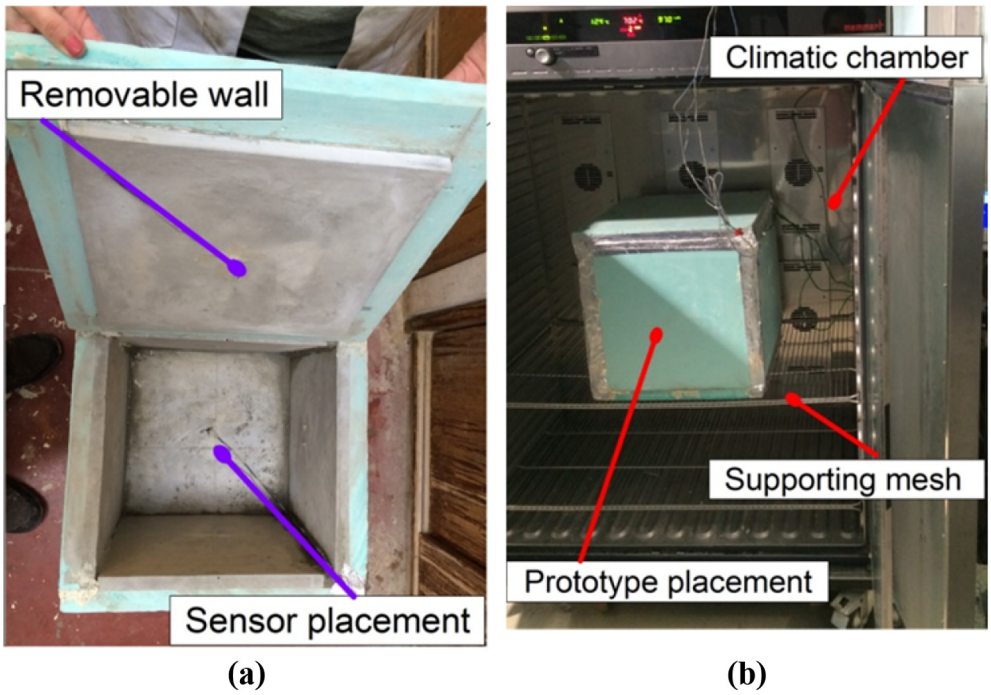

Fig. 5. (a) Photo of the prototype before testing, highlighting the location of the temperature sensor; (b) Prototype within the climatic chamber, ready for testing.

The monitored temperatures during the experimental program for the winter scenario are shown in Fig. 7. It can once more be observed that the thermal amplitudes inside the prototype were lower for the case of HPCMM (4 °C) as compared to REFM (5.6 °C). In order to better interpret the temperature evolution within the HPCMM prototype, the reader is redirected to Fig. 1, where the DSC testing results were plotted: even though the announced melting temperature of RT10 PCM was of 10 °C, its phase change influence is most significantly felt in the range 8°C–16 °C, with particular importance at the vicinity of 14 °C. The monitored temperatures within the HPCMM prototype clearly allow the identification of the phase change activity of RT10 PCM. In fact, relevant heat release can be identified in the points labelled as X1 and X2 in Fig. 7, thus leading the HPCMM prototype to have its lowest temperature increased by 0.6 °C in comparison to the REFM prototype. The converse phase transition of melting (with heat absorption) can also be identified in points Y1 and Y2, identified in Fig. 7, with decrease of the maximum interior temperature of HPCMM prototype by 1 °C in comparison to REFM. However, it should be stressed that, neither REFM nor HPCMM prototypes meet the desirable thermal comfort levels for buildings. This situation would not be acceptable in a real case scenario, where a heating element would be added to the system. Even though such heating element was not included in this research, the increased capacity of HPCMM in attenuating thermal amplitudes as compared to REFM was demonstrated as intended. Further research works of this team will specifically focus on integrating a heating element within the studied prototype and directly evaluate energy savings associated to the inclusion of hybrid PCM mortars.

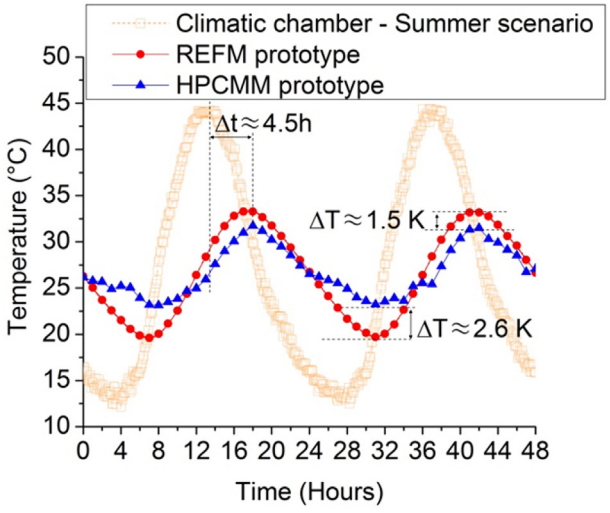

Fig. 6. Monitored temperatures of the prototypes with inner coatings made of HPCMM and REFM under summer scenario.

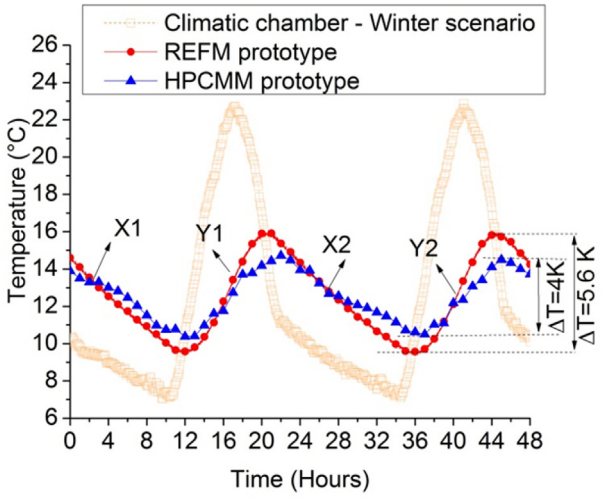

Fig. 7. Monitored temperatures of the prototypes with inner coatings made of HPCMM and REFM under winter scenario.

The overall observations for this winter scenario are similar to those already reported above for summer scenario: the incorporation of PCM leads to a significant attenuation of the amplitude of the effects of the external temperature, with reduction of peak temperatures and an increase in minimum temperatures.

3. Numerical simulation

3.1. Governing equations

The general transient heat balance equation [36] was applied for the numerical treatment of the heat transfer processes in the studied prototypes. All involved materials are considered homogeneous and isotropic. The effect of natural convection due to potential convective flows inside/outside the prototypes was neglected. The feasibility of this simplification was checked through parametric analyses in which natural convection was actually modelled through a computational fluid dynamics approach. It is worth to mention that, the average relative difference between simulations that considered or neglected the effect of natural convection was below 2% for both cases of tested/simulated mortar (REFM and HPCMM). From an engineering point of view, and bearing in mind the intents of this paper, the simplification of neglecting natural convection can thus be considered as plausible. The description of such parametric analyses is omitted here for the sake of brevity. This simplification is nonetheless coherent with criteria already adopted in similar situations by Vaz Sá et al. [25].

Therefore, the heat conduction can be mathematically formulated as a function of time t and the spatial coordinates x, y, z [36]:

$$\rho \times C(T) \times \frac{\partial T}{\partial t} = k \times \left(\frac{\partial^2 T}{\partial x^2} + \frac{\partial^2 T}{\partial y^2} + \frac{\partial^2 T}{\partial z^2} \right) \tag{3}$$

where T is temperature (°C), k is the thermal conductivity of the material (W/m K), $C(T)$ is the temperature dependent specific heat capacity (J/kg K), and ρ is the density of the material (kg/m^3).

In regard to boundary conditions applied to the temperature field computation based on Eq. (3), the corresponding heat flows are taken into account through a convective/radiative boundary flux, as shown in Eq. (4), where T is the temperature (°C), T_s is the surface temperature (°C) and h_{eq} is a convection/radiation coefficient that depends on air speed (W/m K) [37]:

$$q = h_{eq}(T - T_s) \tag{4}$$

3.2. Phase change modelling

Several methods have been used to simulate the latent heat energy release/absorption during phase change processes [16,38]. Lamberg et al. [39] report that computations that consider the effective heat capacity method to simulate the phase change effects have a quite similar performance to those that use the enthalpy method (with slight advantage to the effective heat capacity method). The work reported herein also started by considering both methods and reach similar conclusions of better performance of the effective heat capacity method. For that reason the phase change simulation reported herein shall only adopt the effective heat capacity method. In this basis, phase changes were modelled through a simplified approach by which the energy release/absorption associated to the phase change process is considered through artifacts applied to the specific heat capacity term shown in Eq. (3). This strategy of simulation of the enthalpy of phase change consists in increasing the heat capacity value of the mortar during such process, and is usually termed 'effective heat capacity method' [16]. The computation of the specific heat capacity of the specimen along the tested temperatures $C(T)$(J/g K) is made according to Eq. (5):

$$C(T) = \frac{(DSC(T)_s)}{\varphi} \tag{5}$$

where $DSC(T)_s$ the heat flow across the specimen at temperature T from the thermogram (m W/m g), and φ is the heating rate (°C/s).

It is noteworthy to remark that, in the effective heat capacity method, the sensible heat and latent heat are not distinguishable; therefore, the state of the PCM is not perceptible.

Even though the experimental program did not encompass testing of a prototype containing a single type of PCM embedded, such situation was tackled in the numerical simulation, as to illustrate the performance advantages of the hybrid PCM concept (HPCMM). Therefore, a single PCM mortar, termed as SPCMM will be added to the process of numerical simulations. The single PCM mortar selected for such comparison corresponds to a mix that has been performed and tested in previous works of this research team, which contains 18.34% weight of PCM [13] with melting temperature of 24 °C. It is worth to mention that, such a melting temperature (around 24 °C) is usually used for human thermal comfort purposes [8,40]. Furthermore, three fictitious single PCM mortars made of 18.34% of RT10 (here termed as SPCMM10), BSF26 (here termed as SPCMM26) and MC28 (here termed as SPCMM28) distinctly were also considered for the purpose of comparison in term of energy saving.

As the experimental program did not include the thermal characterization of single PCM mortars, their properties had to be estimated for the numerical simulations. In order to support such estimates, specific DSC experiments were conducted on the relevant PCMs: RT10, MC24, BSF26 and MC28. One specimen per each type of PCM was considered and the weight of the prepared specimens was of 4.185 mg, 5.76 mg, 5.271 mg and 5.126 mg for RT10, MC24, BSF26 and MC28 respectively. The applied program for DSC testing was analogous to those already made for mortars (detailed in section 2.2). The graph of Fig. 8a shows that obtained results are in accordance with the characteristics given by the manufacturers [21–23].

In order to estimate the specific heat capacity curve of single PCM mortars (to be used in the numerical simulations), the method forwarded by Tittelein et al. [41] was utilized. It consists in a proportional mixing law for the specific heat, based on the constituents of the mortar, their weight proportions and their individual specific heat capacities. Therefore, the specific heat capacity of the mortar can be estimated through Eq. (6):

$$C_{specimen} = C_{PCM} \times W_{PCM} + C_{mortar} \times W_{mortar} \tag{6}$$

where $C_{specimen}$ is the specific heat capacity of the specimen (J/kg K); C_{PCM} is the specific heat capacity of the PCM (J/kg K); W_{PCM} weight ratio of the PCM to the specimen; W_{mortar} mass fraction of the plain mortar and C_{mortar} is the specific heat capacity of the plain mortar (J/kg K). Therefore, the specific heat capacities that considered for the mortars are presented in Fig. 8b.

For the particular case of SPCMM, values of relevant properties were obtained from a previous research with this mortar [42]: density of 1360.9 kg/m^3 and thermal conductivity of 0.2 W/m K. And also these values were considered with same quantities for other single PCM mortars with RT10, BSF26 and MC28.

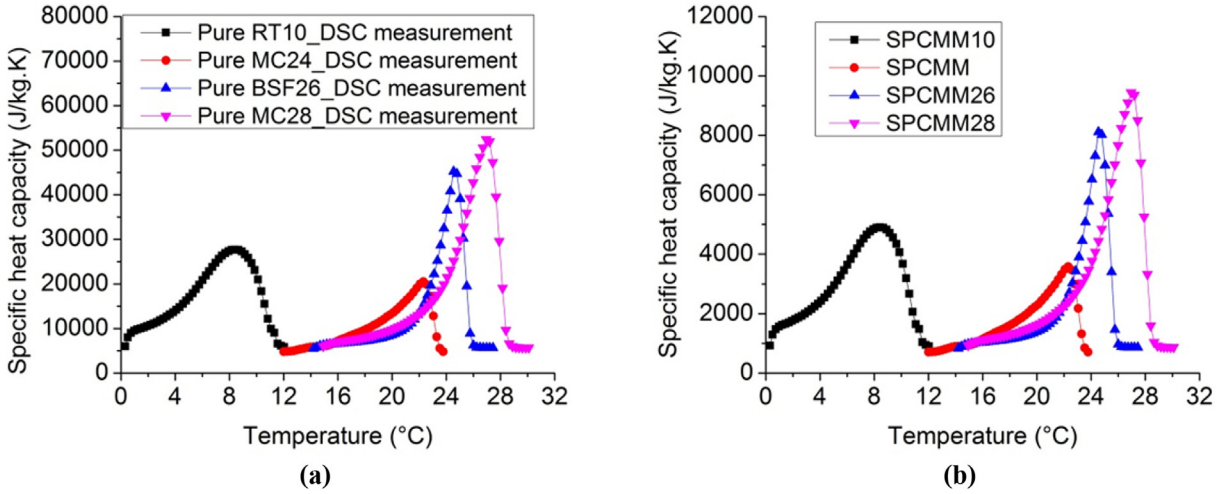

Fig. 8. (a) Specific heat capacities calculated with the DSC outputs for the pure PCM specimens (RT10, MC24, BSF26 and MC28); (b) Estimated specific heat capacity curves of the single PCM mortars.

3.3. Numerical discretization and parameter estimation

The transient heat conduction equation is discretized through the FVM (finite volume method) using ANSYS—FLUENT [43]. Time discretization was handled through a first order scheme.

The computational mesh was built by using hexahedral cells (8 nodes) with typical size of 10^{-6} m^3. A constant time step (Δt) of 300 s was also considered. The grid size and the time step were chosen after careful examination of the independency of the results to these parameters. Taking into account the nonlinearities of the solution process associated to the phase change processes, which induced temperature dependency on the specific heat, specific attention was given to the accuracy of results in such concern. In this way, the energy-based convergence criterion was checked at each time step, with relative variation under 10^{-7} [5,44].

In specific regard to the simulation model of the 0.46 m × 0.46 m × 0.46 m prototype, two vertical symmetry planes were considered, leading to the necessity of solely modelling one fourth of the prototype (0.23 m × 0.23 m × 0.46 m), according to the geometry shown in Fig. 9. The generated finite volume mesh resulted in 25944 cells, depicted in Fig. 9. The exterior top, bottom and lateral surfaces (except for the symmetry planes), were assigned with convective thermal boundary conditions, taking into account the varying temperature imposed in the climatic chamber. As the prototypes were placed inside an indoor climatic chamber, a value ofh_{eq} = 5 W/m K [37] was considered for the surface convection coefficient, in correspondence to near stagnant air conditions. In the symmetry planes, adiabatic boundaries were considered.

It should be mentioned that, the characteristics of the air materials used in the simulation are in correspondence to the air temperature of 24 °C as forwarded: density of 1.225 kg/m^3, specific heat capacity of 1006.43 J/kg K and thermal conductivity of 0.0242 W/m K.

3.4. Results of the numerical simulations

The numerical algorithm was initially validated by comparing its predictions with experimental results available in the literature. The available experimental work by Vaz Sá et al. [25] has been considered to validate the model. Such experimental work encompassed similar small-scale prototypes, which contained a single-PCM mortar. The simulation framework adopted herein is fairly similar, and its validation was achieved by simulating the experiments of Vaz Sá et al. [25], with differences of predicted temperatures below 0.1 °C in comparison to their experimental results. Such confidence in the numerical simulation framework was a cornerstone to the remaining numerical simulations presented in this paper.

The comparison of experimental and simulation results for prototypes with REFM and with HPCMM is shown in Fig. 10 for the summer scenario, and in Fig. 11 for the winter scenario. From observation of both figures, it can be confirmed that the numerical predictions for the $T-t$ evolutions match quite closely the ones measured by the temperature sensor (PT100), within error margins below 0.1 °C. Even though the simulation of the winter scenario was successful, thus adding value to the validation of the simulation framework, no further discussions will be made on such scenario due to the reasons highlighted before, according to which the prototype for winter would need to take into account the existence of heating devices to bring temperatures nearer comfort levels.

Based on the high confidence level provided by the validations mentioned above, a further simulation was carried out for the summer scenario, in which the mortar of the prototype encompassed a single type of PCM with melting temperature of 24 °C (termed SPCMM), with the composition mentioned in section 3.2. The results of such simulation can better assist evaluating the potential benefits that the hybrid PCM concept can bring about. The results of the simulation for SPCMM are included in Fig. 10 for direct comparison of performance with REFM and HPCMM.

Smoother heating/cooling processes are exhibited for the cases in which PCM-based mortars are used (both HPCMM and SPCMM) in comparison to the reference mortar.

As it can be seen in Fig. 10, the maximum peak temperatures are reached with about 4.5 h delay in comparison to the maximum peak in the climatic chamber, regardless of the fact that the mortar has PCM or not. Furthermore, the minimum temperatures are reached with delays of nearly 3 h, 4 h and 5.5 h for the cases of REFM, HPCMM and SPCMM compared with the minimum environmental temperature respectively. Minimum temperatures in the SPCMM and HPCMM are nearly 2 °C and 2.5 °C higher than in the REFM case.

It is interesting to note that, heating and cooling processes are smoother for the HCPMM prototype than for the simulated SPCMM prototype. The reason might be due to the existence of a wider phase change domain in the case of HPCMM (between 2 °C and

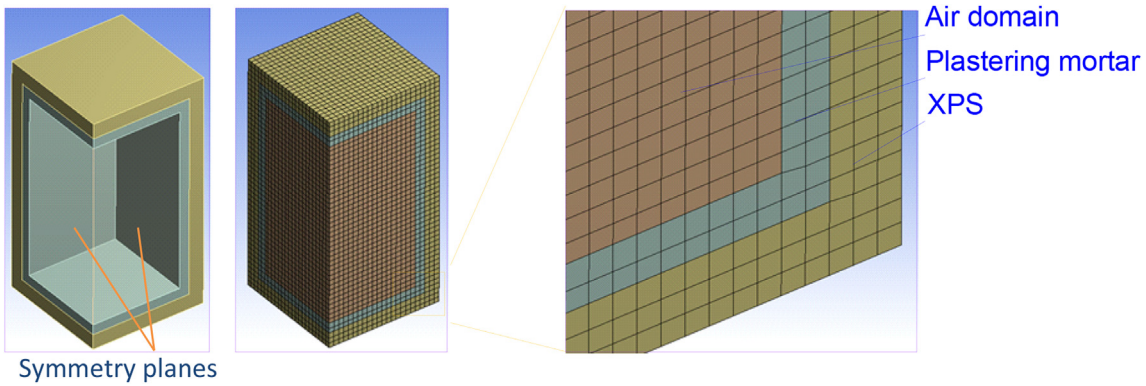

Fig. 9. –The 3D geometric model, model mesh and zoomed mesh.

29 °C as shown in Fig. 1), as compared to the narrow domain of actuation of MC24 seen in Fig. 8 (approximately ranging from 12 °C to 24 °C).

The surface temperature of internal walls is one of the most important thermal comfort parameters in a room [45]. The following analysis shows the effects of latent heat storage on the thermal behaviour of the internal plastering mortar.

To better understand the PCM action, Fig. 12 compares the simulated temperature evolution at mid-depth of the mortar layer for both the HPCMM and REFM prototypes under summer and winter scenarios with the corresponding external environmental temperature. In this figure, the relevant phase change domain temperatures of the PCMs present in HPCMM are signalled with a shaded region: (i) for the summer scenario, the shaded region ranges 20.5°C–27.5 °C corresponding respectively to the onset temperature of BSF26 and the end temperature of the MC28; (ii) for the winter scenario, the shaded region ranges 9°C–16 °C, corresponding to the onset and end temperatures of RT10. Fig. 12a,b shows that the internal mortar temperature (labelled as P) for HPCMM keeps within its phase change domain for about 67% and 100% of the time of each daily cycle, respectively. This is a clear indication that the capacity to store/release energy of the PCMs present in the mortar is being constantly or almost constantly deployed, in correspondence to an adequate design of the hybrid PCM blend.

For further illustration of the effect of PCM in the mortar, Fig. 13 shows the calculated temperature profile in the wall layer of the HPCMM prototype at several instants within a given daily cycle (summer scenario). The selected instants that range 1 h–15 h show that the HPCMM layer is enduring a quasi-isothermal state at such stage (attained by latent heat storage/release), while the temperatures in the outer XPS layer keep oscillating with significant gradients, according to the outer environmental temperature [9]. Naturally, this capacity is manifested within the relevant melting ranges of the PCMs present in the mortar, as identified by horizontal dashed lines in Fig. 13: onset temperature of 20.5 °C for BSF26 and end temperature of 27.5 °C for MC28. Similar findings/conclusions can be attained by analysis of the winter situation.

The potential to save energy induced by the presence of hybrid PCM materials may be discussed with basis on the observation of the various temperature evolutions. In some studies [46,47], the calculation of accumulated energy was performed based on heat flux measurements. However, in the absence of heat flux measurements, this work relies on a simplified approach that can provide indirect information about energy savings for cooling. The process is quite simple and it is illustrated in Fig. 14. First, a maximum threshold temperature for comfort was established as 26 °C for the summer scenario, in coherence with the recommendations of ASHRAE [48]. When the temperature within the studied prototype overcomes this threshold, the internal environment is

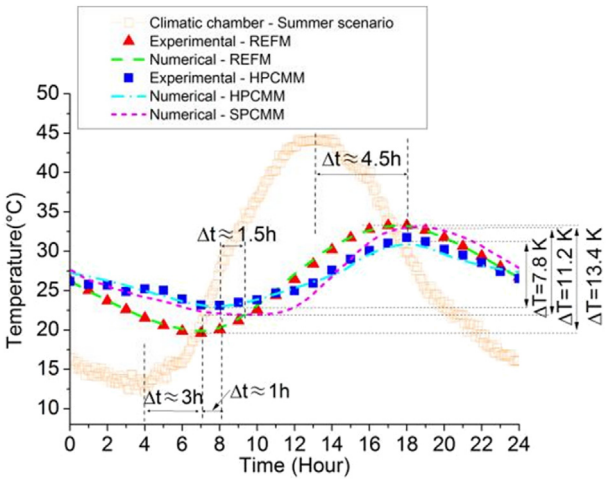

Fig. 10. Experimental versus numerical values for test cells REFM and HPCMM (Summer scenario).

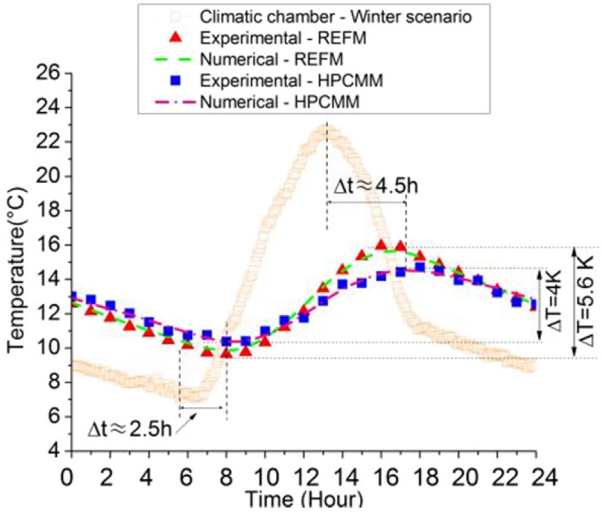

Fig. 11. Experimental versus numerical values for test cells REFM and HPCMM (winter scenario).

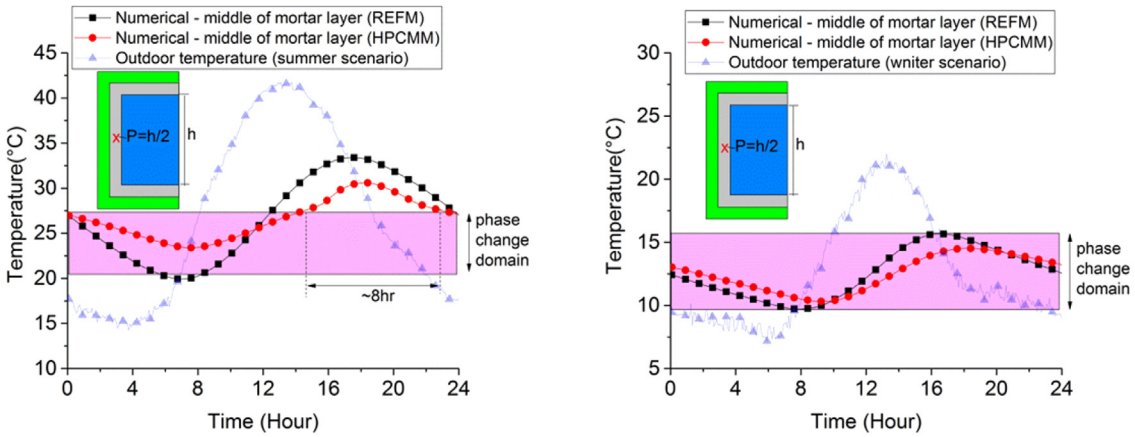

Fig. 12. Simulation of evolution of temperature at mid-depth of the mortar layer (labelled as P) for both REFM and HPCMM prototypes: (a) summer scenario; (b) winter scenario.

considered to be within a discomfort period, and a penalty function is calculated by integrating the time–temperature diagram with the baseline of the threshold temperature (shaded Region A in Fig. 14). The global value of such penalty function for a full daily cycle is expressed as the TT index (units: °C h). This TT index can be used as a comparative performance indicator in terms of cooling needs: the higher the index, the higher the cooling energy demands are.

The results of the calculated TT index are shown in Fig. 15. These results reveal that, in the tested summer day, the HPCMM mortar is clearly the best-performing material in terms of thermal comfort and potential energy savings. Indeed, it outperforms any of the other alternatives by more of 50% reduction in TT. It is also interesting to note that inadequate selection of PCM can bring even worse behaviour as compared to REFM. This is the case of SPCMM10 and SPCMM (includes MC24). The reason for this decreased behaviour is that the phase change of both these PCMs (ranges of operation identified in Fig. 8) is never mobilized with the sol-air temperature that is being imposed to the prototype (see Fig. 4), and also because the volumetric specific heat of SPCMM10 and SPCMM is smaller than that of REFM.

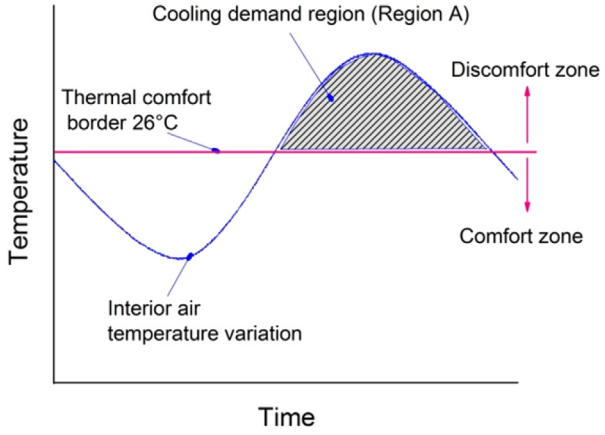

Fig. 14. Theoretical bases of temperature along time strategy with respect to the thermal comfort level during a cycle (includes a day and a night).

4. Conclusions

In this paper, a set of experiments and numerical simulations were performed in order to demonstrate the transient thermal

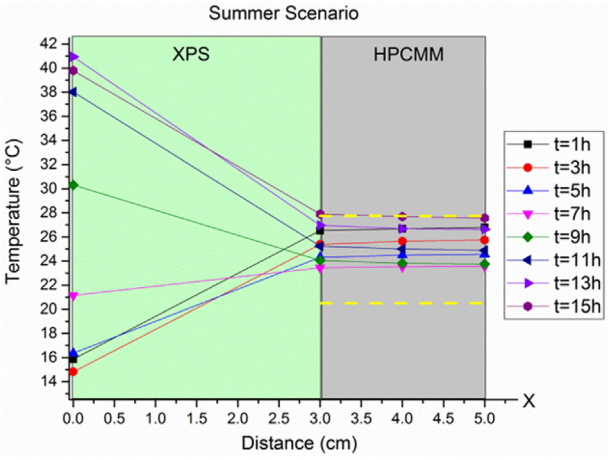

Fig. 13. Temperature variations along the thickness of the wall of HPCMM prototype at different hours in summer scenario.

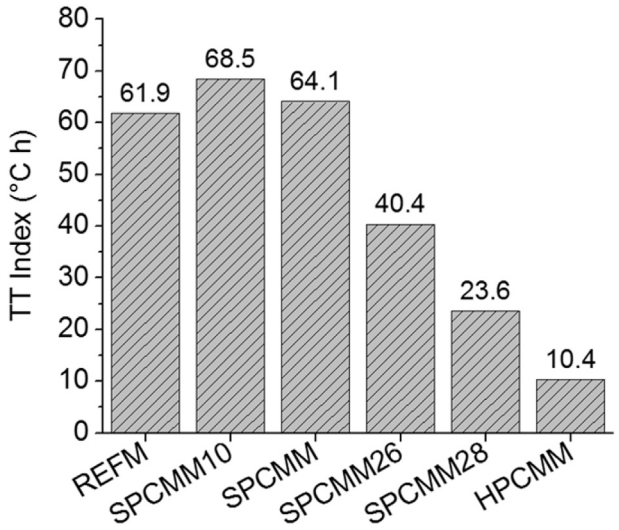

Fig. 15. Comparison between different cases on the total required cooling temperature through time (based on calculation of region A) in order to turn the temperature at comfort level.

behaviour of plastering mortars containing hybrid PCM blends, as compared to the behaviour of regular mortars, or those containing a single type of PCM. After an initial round of characterization of the materials involved in the experimental program, laboratory scale prototypes that consisted in hollow boxes rendered with the mortars under test, were deployed as to evaluate the capacity of the tested mortars in effecting inner temperatures of the prototypes themselves. Two prototypes, containing REFM (respectively a reference mortar) and a mortar containing and hybrid blend of embedded PCMs (HPCMM), where submitted to realistic daily temperature cycles and inner temperatures were recorded. Finally, a set of numerical simulations of the thermal behaviour of the prototypes was performed through the finite volume analyses method, aiming validation of simulation capacity, but also for further sensitivity analysis of test situations that were not experimentally assessed.

From the conducted research the following main conclusions were obtained:

1) The prototype rendered with HPCMM allowed a much stronger attenuation of the external thermal amplitudes on its interior, as compared to the situation of the REFM prototype. This situation was observed in both summer and winter scenarios.
2) The adopted framework for numerical simulation has shown adequate predictive capacity by reproducing the experimental results of all experiments with an error margin that was always below 0.1 °C. This validation of simulation capabilities provided grounds for the conduction of further simulations for sensitivity analyses.
3) Based on the set of experiments and simulations, it was also inferred that the utilization of hybrid PCM blends has revealed the capacity to better attenuate daily environmental thermal amplitudes within the test cells for both summer and winter scenarios as compared to any of the other studied alternatives (reference mortars or single PCM mortars). Indeed the combination of several PCMs with melting points that cover a large range of temperatures allow this solution to be advantageous in a much broader sense than classical single PCM approaches that tend to have a more limited scope of activation and usefulness. It could even be demonstrated that a bad choice of PCM melting points in a given blend can even induce worse behaviour than that which would be expectable in a traditional mortar.
4) Even though direct conclusions could be obtained in regard to the potential of cooling energy saving harvested by the use of hybrid PCM blends in the summer scenario (using the TT index), no direct conclusions can be taken for the winter scenario. Indeed the winter experiments/simulations just allowed demonstrating that the hybrid PCM mortar still outperforms the reference mortar in reducing internal thermal amplitudes inside the prototype. However, the range of internal temperatures in the prototype was unrealistically low as compared to the desirable thermal comfort ranges. Therefore, in order to obtain more definite conclusions in this concern, new further experiments are being deployed, in which an internal heater is placed in the prototypes, and the performance assessment in winter scenarios is made directly through the energy savings in heating as to maintain internal temperature within acceptable comfort limits.

As a final note, it is pointed that the concept of blending more than one type of PCM into plastering mortars has revealed promising performance capacity. The up scaling of this concept is bound to bring added value to thermal performance of buildings. Indeed, by being able adequately predict the behaviour of such blends of PCMs in the scope of real buildings, it will be possible to tailor the optimum blends for specific needs, both in terms of façade orientation, but also regarding the building location as a whole.

Acknowledgements

The authors would like to acknowledge the financial support of the Foundation for Science and Technology (FCT) in the frame of: (i) project CENTRO-07-ST24_FEDER-002020; (ii) project PTDC/ECM/102154/2008; (iii) C-TAC, ISISE and C–MADE research units.

References

[1] Hembade L, Neithalath N, Rajan S. Understanding the energy implications of phase-change materials in Concrete Walls through finite-element analysis. J Energy Eng 2014;140(1):04013009.
[2] IEA (International Energy Agency). Energy balances of OECD countries—2010 edition. 2010. Paris, France.
[3] Soares N, Costa JJ, Gaspar AR, Santos P. Review of passive PCM latent heat thermal energy storage systems towards buildings' energy efficiency. Energy Build 2013;59:82–103.
[4] Madenci E, Guven I. The finite element method and applications in engineering using ANSYS®. Springer; 2015.
[5] Wang Y-H, Yang Y-T. Three-dimensional transient cooling simulations of a portable electronic device using PCM (phase change materials) in multi-fin heat sink. Energy 2011;36(8):5214–24.
[6] Jin X, Zhang X. Thermal analysis of a double layer phase change material floor. Appl Therm Eng 2011;31(10):1576–81.
[7] Joulin A, Zalewski L, Lassue S, Naji H. Experimental investigation of thermal characteristics of a mortar with or without a micro-encapsulated phase change material. Appl Therm Eng 2014;66(1–2):171–80.
[8] Jaworski M. Thermal performance of building element containing phase change material (PCM) integrated with ventilation system – an experimental study. Appl Therm Eng 2014;70(1):665–74.
[9] Vicente R, Silva T. Brick masonry walls with PCM macrocapsules: an experimental approach. Appl Therm Eng 2014;67(1–2):24–34.
[10] Song S, Dong L, Zhang Y, Chen S, Li Q, Guo Y, et al. Lauric acid/intercalated kaolinite as form-stable phase change material for thermal energy storage. Energy 2014;76:385–9.
[11] Cunha S, Aguiar J, Pacheco-Torgal F. Effect of temperature on mortars with incorporation of phase change materials. Constr Build Mater 2015;98:89–101.
[12] Ling T-C, Poon C-S. Use of phase change materials for thermal energy storage in concrete: an overview. Constr Build Mater 2013;46:55–62.
[13] Cunha S, Aguiar J, Ferreira V, Tadeu A. Mortars based in different binders with incorporation of phase-change materials: physical and mechanical properties. Eur J Environ Civ Eng 2015;19(10):1216–33.
[14] Jeong S-G, Jeon J, Cha J, Kim J, Kim S. Preparation and evaluation of thermal enhanced silica fume by incorporating organic PCM, for application to concrete. Energy Build 2013;62:190–5.
[15] Haurie L, Mazo J, Delgado M, Zalba B. Fire behaviour of a mortar with different mass fractions of phase change material for use in radiant floor systems. Energy Build 2014;84:86–93.
[16] Al-Saadi SN, Zhai Z. Modeling phase change materials embedded in building enclosure: a review. Renew Sustain Energy Rev 2013;21:659–73.
[17] Kheradmand M, Azenha M, de Aguiar JLB, Krakowiak KJ. Thermal behavior of cement based plastering mortar containing hybrid microencapsulated phase change materials. Energy Build 2014;84(0):526–36.
[18] The World Weather Online. Global weather forecast and weather content for websites businesses and the travel industry. 2014. http://www.worldweatheronline.com [retrieved 2014].
[19] Park S, Lee Y, Kim YS, Lee HM, Kim JH, Cheong IW, et al. Magnetic nanoparticle-embedded PCM nanocapsules based on paraffin core and polyurea shell. Colloids Surfaces A Physicochem Eng Aspects 2014;450(0):46–51.
[20] Tyagi VV, Buddhi D. PCM thermal storage in buildings: a state of art. Renew Sustain Energy Rev 2007;11(6):1146–66.
[21] Devan Chemicals. THERMIC temperature regulation technology. Portugal. 2012.
[22] BASF Micronal. PCM intelligent temperature management for buildings. 2012.
[23] Rubitherm GmbH. Technologies is the leading manufacturer of innovative phase change material – RT. Germany. 2012.
[24] EN 1015-3. Methods of test for mortar for masonry. Determination of consistence of fresh mortar (by flow table). 1999.
[25] Vaz Sá A, Azenha M, de Sousa H, Samagaio António. Thermal enhancement of plastering mortars with phase change materials: experimental and numerical approach. Energy Build 2012;49:16–27.
[26] FIBRANs Energy Shield. Thermal insulation with extruded polystyrene. 2011. http://www.fibran.com/frontend/index.php.
[27] EN1015–10. E. Standard (CEN). In: Methods of test for mortar for masonry; 2006.
[28] ISO:8301. Thermal insulation: determination of steady state thermal resistance and related properties, heat flow meter apparatus. 1991.
[29] Lecompte T, Le Bideau P, Glouannec P, Nortershauser D, Le Masson S. Mechanical and thermo-physical behaviour of concretes and mortars containing phase change material. Energy Build 2015;94(0):52–60.

[30] EN ISO 11357–1. Plastics – differential scanning calorimetry (DSC) Part 1: General principles. Berlin: DIN Deutsches Institut für Normung e.V.; 1997.
[31] Biswas K, Lu J, Soroushian P, Shrestha S. Combined experimental and numerical evaluation of a prototype nano-PCM enhanced wallboard. Appl Energy 2014;131(0):517–29.
[32] Kousksou T, Jamil A, Zeraouli Y. Enthalpy and apparent specific heat capacity of the binary solution during the melting process: DSC modeling. Thermochim Acta 2012;541(0):31–41.
[33] Pomianowski M, Heiselberg P, Jensen RL. Dynamic heat storage and cooling capacity of a concrete deck with PCM and thermally activated building system. Energy Build 2012;53(0):96–107.
[34] RCCTE. Regulamento das Características de Comportamento Térmico dos Edifícios (RCCTE). 2006.
[35] ISO6946. Building components and building elements-Thermal resistance and thermal transmittance- calculation method. 2007.
[36] Incopera F, Dewitt D, Bergman T, Lavine A. Fundamentals of heat and mass transfer. John Wiley; 2007.
[37] Azenha M. Numerical simulation of the structural behaviour of concrete since its early ages [PhD thesis]. University of Porto; 2009.
[38] Zhang Y, Du K, Medina MA, He J. An experimental method for validating transient heat transfermathematical models used for phase change materials(PCMs) calculations. Phase Transitions 2014;87(6):541–58.
[39] Lamberg P, Lehtiniemi R, Henell A-M. Numerical and experimental investigation of melting and freezing processes in phase change material storage. Int J Therm Sci 2004;43(3):277–87.
[40] Evola G, Marletta L, Sicurella F. Simulation of a ventilated cavity to enhance the effectiveness of PCM wallboards for summer thermal comfort in buildings. Energy Build 2014;70:480–9.
[41] Tittelein P, Gibout S, Franquet E, Johannes K, Zalewski L, Kuznik F, et al. Simulation of the thermal and energy behaviour of a composite material containing encapsulated-PCM: Influence of the thermodynamical modelling. Appl Energy 2015;140(0):269–74.
[42] Kheradmand M, Barroso de Aguiar J, Azenha M. Assessment of the thermal performance of plastering mortars within controlled test cells CLB-MCS. Guimaraes, Portugal: University of Minho; 2014.
[43] ANSYS Inc.-FLUENT. http://www.ansys.com/. User's guide, Release 14.5.
[44] Kashani S, Ranjbar AA, Abdollahzadeh M, Sebti S. Solidification of nano-enhanced phase change material (NEPCM) in a wavy cavity. Heat Mass Transf 2012;48(7):1155–66.
[45] Catalina T, Virgone J, Kuznik F. Evaluation of thermal comfort using combined CFD and experimentation study in a test room equipped with a cooling ceiling. Build Environ 2009;44(8):1740–50.
[46] Sayyar M, Weerasiri RR, Soroushian P, Lu J. Experimental and numerical study of shape-stable phase-change nanocomposite toward energy-efficient building constructions. Energy Build 2014;75:249–55.
[47] Kuznik F, Virgone J. Experimental investigation of wallboard containing phase change material: data for validation of numerical modeling. Energy Build 2009;41(5):561–70.
[48] ASHRAE55. Thermal environment standards for human occupancy. 55. 2004. Atlanta, GA.